PERGAMON

International Journal of Solids and Structures 36 (1999) 1541–1556

INTERNATIONAL JOURNAL OF SOLIDS and STRUCTURES

A finite element model of ferroelastic polycrystals

Stephen C. Hwang[a], Robert M. McMeeking[a,b,*]

[a] *Materials Department, College of Engineering, University of California, Santa Barbara, CA 93106-5050, U.S.A.*
[b] *Mechanical and Environmental Engineering, College of Engineering, University of California, Santa Barbara, CA 93106-5050, U.S.A.*

Received 7 October 1997; in revised form 22 January 1998

Abstract

A finite element model of switching in polycrystalline ferroelastic ceramics is developed. It is assumed that a crystallite switches if the reduction in mechanically driven potential energy of the system exceeds a critical value per unit volume of switching material. Stress induced (i.e. ferroelastic) switching is a change of permanent strain in characteristic crystallographic directions. Martensitic twinning is one example, but the strain response of ferroelectric materials has the same characteristics. The model is suitable for representing ferroelastic systems such as shape memory alloys and as a preliminary model for ferroelectric/ferroelastic materials such as perovskite piezoelectrics. In the simulations, each crystallite is represented by a finite element and the crystallographic principal direction for each crystallite is assigned randomly. Different critical values for the energy barrier to switching are selected to simulate stress vs strain hysteresis loops of a ceramic lead lanthanum zirconate titanate (PLZT) at room temperature. The measured stress versus strain curves of polycrystalline ceramics designated PZT-A and PZT-B are also reproduced by the model. © 1998 Elsevier Science Ltd. All rights reserved.

1. Introduction

Ferroelectric materials (Jaffe et al., 1971) such as lead zirconate titanate (PZT) and lead lanthanum zirconate titanate (PLZT) experience a polarization switch at the unit cell level when a sufficiently large electric field is applied in a direction orthogonal to the current poling. This switch involves the reorientation of the tetragonality (or other relevant reorientations for non-tetragonal crystallographies) of the unit cell containing the electrical dipoles. As a result, there is a strain change in general during repolarization and it follows that the material is also ferroelastic. This means that an appropriately oriented applied stress of sufficient magnitude will also induce the strain change because it can also cause the reorientation of the tetragonality of the unit cells.

When stress alone drives the switching process, no net polarization can be created because the

* Corresponding author. Fax: 8058938651; e-mail: rmcm@ecil.ucsb.edu

0020–7683/99/$ - see front matter © 1998 Elsevier Science Ltd. All rights reserved
PII: S0020–7683(98)00051–1

dipoles randomly align in positive and negative directions. Thus polarization can be destroyed by stress but no created. Consequently, a polycrystalline ferroelectric sample with random initial polarization in its domains will remain unpolarized after the application of stress alone. As a result, an initially unpolarized polycrystalline ferroelectric ceramic can be treated as a purely mechanical ferroelastic element with the effect of internal electric fields and polarizations neglected. This approach represents an approximate model for the deformation of ferroelectric polycrystals subjected to stress alone because the local internal electric fields and polarizations will have some effect on the processes by which switches take place. However, it is a useful step to consider the ferroelastic behavior alone in the modeling of the deformation of ferroelectric polycrystals subjected to stress in the absence of electric field.

When considered as a purely ferroelastic material, the behavior of ferroelectric polycrystals is very similar to that of shape memory alloys (Duerig et al., 1990). In the latter case, the process of twinning and detwinning of the martensitic phase is analogous to the process of switching in ferroelectric materials. Parallels can also be drawn between behavior in ferroelectrics and stress induced martensitic phase transformations in shape memory alloys and in other materials such as zirconia (McMeeking and Evans, 1982).

It is of interest to model the behavior of these materials at the mesoscopic level. That is, models for the switching of individual domains or crystallites can be used in conjunction with analysis of the internal mechanical stresses and deformations which are induced as a result of those switches. In such a way, models for the average ferroelastic behavior of polycrystalline aggregates can be developed. These models can be used to predict the deformation of polycrystalline aggregates in response to completely general states of stress. Consequently, they can give insights additional to those provided by experiments and can provide guidance in the development of concise constitutive laws for use in, say, design calculations for ferroelectrics and shape memory alloys. Initial work using elementary approximate methods has been carried out (Chan and Hagood, 1994; Hwang et al., 1995; Hwang and McMeeking, 1998). More exact methods can be introduced, such as treatments using the finite element method and that is the purpose of this paper and another in which we have treated the purely electrical effects of ferroelectric switching (Hwang and McMeeking, 1998).

The finite element method used for this paper treats each crystallite as an element with uniform crystallography, with the tetragonal orientation for each element selected randomly. When switching occurs for a given element, the tetragonal axis changes to a different permitted direction. The governing equations of compatibility and mechanical equilibrium are enforced through the finite element equations. Thus, the effect of local incompatibilities among crystallites is allowed for and local stresses arising as a result are computed. This is significant because a major drawback in a high-strain actuator application of ferroelectric materials is microcracking (i.e. grain size cracks forming at the grain boundaries) and debonding at the metal electrode–ceramic layer interface (Aburatani et al., 1994), both caused by high local stresses. The mechanism of cracking is due to domain reorientations (Jiang et al., 1994; Wang et al., 1996). The finite element model is developed to be also useful as a tool for understanding material degradation mechanisms in fatigue and fracture (Jiang et al., 1994; Wang et al., 1996; Park and Sun, 1995).

It is assumed that each crystallite in the ceramic is tetragonal (e.g. PZT) with three possible orthogonal orientations for the c-axis. Only displacement and strain are computed in this paper with no electric field or electrical polarization involved. The finite element calculations are carried

out with a large number of crystallites having initially random tetragonality. Each finite element is a crystallite which is assumed to be a single domain, or set of cooperating domains, switching all at once when the transformation takes place. The starting point for the simulations is therefore one of zero macroscopic strain. The mechanical load is then gradually increased and later reversed. An individual crystallite is allowed to switch when the potential energy of the system will reduce by a critical amount as a result of that switch. The reduction of potential energy is considered to be necessary to overcome barriers opposing the transformation. The behavior is followed incrementally by permitting the switching of the most favored element in each step. The load is kept constant after each step until all the energetically favorable elements switch. After all such elements have switched, the load is then incremented once more.

The parameters of the model are chosen from empirical constants of a lead lanthanum zirconate titanate (PLZT 8/65/35) ceramic. Several simulated results with selected values for the energy barrier to switching are presented. Among the results, the best fit compared to an experimental measurement of a stress vs longitudinal strain curve is obtained. Then, new parameters are chosen to reproduce the stress vs strain curves of hard PZT-A and soft PZT-B ceramics as measured by Cao and Evans (1993).

2. Governing equations

A ferroelastic ceramic is considered to be purely mechanical without body force. Tractions are specified on an arbitrary part S_T of the external perimeter S of the body. For a volume V, equilibrium requires

$$\partial\sigma_{ij}/\partial x_i = 0 \tag{1}$$

where σ is the mechanical stress and x is position. Continuity of stress at crystallite boundaries requires that

$$n_i[|\sigma_{ij}|] = 0 \tag{2}$$

where n is the unit normal to the interface and the symbol $[|\ |]$ denotes a jump of the quantity within. The elasticity law for a given crystallite is

$$\sigma_{ij} = C_{ijkl}(e_{kl} - e^s_{kl}) \tag{3}$$

where C is the elastic tensor, e is the strain, and e^s is the tensor of spontaneous strain for that crystallite. The datum for the spontaneous strain is taken to be a cubic state having the same volume. The strain tensor e is defined by

$$e_{ij} = (\partial u_i/\partial x_j + \partial u_j/\partial x_i)/2 \tag{4}$$

where u is the displacement vector.

3. Energy relationships and switching criterion

The potential energy of a ferroelastic ceramic is given by (McMeeking and Hwang, 1997)

$$\Omega[u] = \frac{1}{2}\int_v (e_{ij} - e^{\mathrm{s}}_{ij}) C_{ijkl} (e_{kl} - e^{\mathrm{s}}_{kl})\, \mathrm{d}V - \int_{S_\mathrm{T}} T_i u_i \, \mathrm{d}S \tag{5}$$

The first integral is the recoverable elastic energy stored in the material and the second is the potential energy of the traction T specified on the part S_T of the boundary S. A crystallite is assumed to switch when the resulting change of the potential energy of the ceramic $\Delta\Omega[u]$ is equal to or larger than the energy barrier for the switch. Thus, the switching criterion is given by

$$\Delta\Omega[u] + V_\mathrm{c}\Delta\psi_\mathrm{c} \leqslant 0 \tag{6}$$

where $\Delta\psi_\mathrm{c}$ is the energy barrier per unit volume of a crystallite which must be overcome upon switching. Only the most favorable crystallite is allowed to switch at any stage and only one is permitted to switch at any time. All other crystallites (particularly neighboring ones) elastically accommodate the switch at that instant. This is, perhaps, unrealistic since multiple domains could, in principle, switch simultaneously. However, this model has been adopted as a first attempt given that consideration of multiple switching is computationally impractical since too many combinations have to be considered.

When a switch take place, the imposed traction T is held fixed, but the spontaneous strain of the crystalline changes to a new value, $e^{\mathrm{s}} + \Delta e^{\mathrm{s}}$. Upon switching, the magnitude of the spontaneous strain, e^{s}, remains the same whereas its principal directions change, effectively to align the crystallite tetragonality as closely as possible to the internal stress in the crystallite. Due to the change of the spontaneous strain and the elastic adjustments to the switch, the strain of the ceramic becomes a new value $e + \Delta e$ and correspondingly the displacement becomes $u + \Delta u$. The change of the energy in the system $\Delta\Omega[u]$ is given by

$$\Delta\Omega[u] = \int_V (e_{ij} - e^{\mathrm{s}}_{ij}) C_{ijkl} (\Delta e_{kl} - \Delta e^{\mathrm{s}}_{kl})\, \mathrm{d}V + \frac{1}{2}\int_V (\Delta e_{ij} - \Delta e^{\mathrm{s}}_{ij}) C_{ijkl} (\Delta e_{kl} - \Delta e^{\mathrm{s}}_{kl})\, \mathrm{d}V - \int_{S_\mathrm{T}} T_i \Delta u_i \, \mathrm{d}S \tag{7}$$

where it is assumed that the elastic moduli are unaffected by the switch tetragonality. This is not the most general situation, but is used as an initial model. Since the stress

$$\sigma_{kl} = C_{ijkl}(e_{ij} - e^{\mathrm{s}}_{ij}) \tag{8}$$

in V is in equilibrium with the traction T everywhere on S and the displacements Δu are zero on $S - S_\mathrm{T}$ and are compatible with the strain Δe in V, virtual work provides

$$\int_V (e_{ij} - e^{\mathrm{s}}_{ij}) C_{ijkl} \Delta e_{kl}\, \mathrm{d}V = \int_{S_\mathrm{T}} T_i \Delta u_i \, \mathrm{d}S \tag{9}$$

As a result, eqn (7) simplifies to

$$\Delta\Omega[u] = -\int_V \Delta e^{\mathrm{s}}_{ij}\sigma_{ij}\,\mathrm{d}V + \int_V \left(\frac{1}{2}\Delta e_{ij}C_{ijkl}\Delta e_{kl} - \Delta e^{\mathrm{s}}_{ij}C_{ijkl}\Delta e_{kl} + \frac{1}{2}\Delta e^{\mathrm{s}}_{ij}C_{ijkl}\Delta e^{\mathrm{s}}_{kl}\right)\mathrm{d}V \tag{10}$$

The stress increment

$$\Delta\sigma_{kl} = C_{ijkl}(\Delta e_{ij} - \Delta e^{\mathrm{s}}_{ij}) \tag{11}$$

in V is in equilibrium with the increment of traction ΔT on S. The strain increment Δe in V is compatible with the displacement increment Δu on S. The traction increment is zero on S_{T} whereas the displacement increment is zero on $S - S_{\mathrm{T}}$. Therefore, virtual work gives

$$\int_V (\Delta e_{ij} - \Delta e^{\mathrm{s}}_{ij})C_{ijkl}\Delta e_{kl}\,\mathrm{d}V = 0 \tag{12}$$

so that finally

$$\Delta\Omega[u] = -\int_V \Delta e^{\mathrm{s}}_{ij}\sigma_{ij}\,\mathrm{d}V + \frac{1}{2}\int_V \Delta e^{\mathrm{s}}_{ij}C_{ijkl}\Delta e^{\mathrm{s}}_{kl}\,\mathrm{d}V - \frac{1}{2}\int_V \Delta e_{ij}C_{ijkl}\Delta e_{kl}\,\mathrm{d}V \tag{13}$$

4. Finite element method

The basic field equations for a finite element method can be developed from the principle of virtual work

$$\int_V \delta e_{ij}\sigma_{ij}\,\mathrm{d}V = \int_S \delta u_i T_i\,\mathrm{d}S \tag{14}$$

where $\delta(\cdot)$ indicates a virtual variation. The boundary conditions are

$$\begin{aligned} n_i\sigma_{ij} &= T^0_j \quad \text{on } S_{\mathrm{T}} \\ u_i &= u^0_i \quad \text{on } S_{\mathrm{u}} \end{aligned} \tag{15}$$

where T^0 is given on S_{T} and u^0 is given on S_{u} with $S_{\mathrm{u}} + S_{\mathrm{T}} = S$. In a matrix notation, the displacement components of u can be written in terms of finite element interpolations as

$$\begin{Bmatrix} u_1 \\ u_2 \\ u_3 \end{Bmatrix} = [N]\{u_N\} \tag{16}$$

where the matrix $[N]$ contains interpolation functions and the vector $\{u_N\}$ contains the displacements for all the nodal points in the finite element mesh (Cook et al., 1989). The strain for each element in $\{e\}$ is given in a column vector as

$$\{e_{11} \quad e_{22} \quad e_{33} \quad 2e_{23} \quad 2e_{13} \quad 2e_{12}\}^{\mathrm{T}} = \{e\} = [B]\{u_N\} \tag{17}$$

where the interpolation matrix $[B]$ results from differentiation of $[N]$. In discretized form, eqn (14) becomes

$$\int_V [B]^{\mathrm{T}}\{\sigma\}\,\mathrm{d}V = \int_S [N]^{\mathrm{T}}\{T\}\,\mathrm{d}S \tag{18}$$

where $\{\sigma\}$ is a column vector containing stress components in the same order as in $\{e\}$, $\{T\}$ is $\{T_1\ T_2\ T_3\}^{\mathrm{T}}$ and the superscript T stands for the transpose of a matrix or vector. The requirement that eqn (14) must be true for all virtual variations of nodal displacements has been used to eliminate $\{\delta u_N\}$. Use of the constitutive law eqn (3) then gives the finite element equations

$$[K]\{u_N\} = \{F\} + \{F^{\mathrm{s}}\} \tag{19}$$

where $[K]$ is the stiffness matrix, $\{F\}$ is the nodal load due to the tractions T on S, and $\{F^{\mathrm{s}}\}$ is the additional nodal load due to the spontaneous strain. The stiffness matrix $[K]$ and column vectors $\{F\}$ and $\{F^{\mathrm{s}}\}$ are given as

$$\begin{aligned}
[K] &= \int_V [B]^{\mathrm{T}}[C][B]\,\mathrm{d}V \\
\{F\} &= \int_S [N]^{\mathrm{T}}\{T\}\,\mathrm{d}S \\
\{F^{\mathrm{s}}\} &= \int_V [B]^{\mathrm{T}}[C]\{e^{\mathrm{s}}\}\,\mathrm{d}V
\end{aligned} \tag{20}$$

where $[C]$ is the matrix of linear elastic constants such that

$$\{\sigma\} = [C](\{e\} - \{e^{\mathrm{s}}\}) \tag{21}$$

In discretized form, the change of potential energy due to switching from eqn (13) is

$$\Delta\Omega[u] = -\int_V \{\Delta e^{\mathrm{s}}\}^{\mathrm{T}}\{\sigma\}\,\mathrm{d}V + \frac{1}{2}\int_V \{\Delta e^{\mathrm{s}}\}^{\mathrm{T}}[C]\{\Delta e^{\mathrm{s}}\}\,\mathrm{d}V - \frac{1}{2}\{\Delta u_N\}^{\mathrm{T}}[K]\{\Delta u_N\} \tag{22}$$

The increments of nodal displacements $\{\Delta u_N\}$ caused by the switch must satisfy the finite element equations

$$[K]\{\Delta u_N\} = \{\Delta F^{\mathrm{s}}\} \tag{23}$$

which are modified for incremental form from eqn (19). Since the tractions are held fixed during a switch, only the nodal force increments from the switching term appear on the right hand side of eqn (23). This term is given from eqn (20) by

$$\{\Delta F^{\mathrm{s}}\} = \int_V [B]^{\mathrm{T}}[C]\{\Delta e^{\mathrm{s}}\}\,\mathrm{d}V \tag{24}$$

4.1. Numerical simulation

The model for the ferroelastic switching behavior is implemented in a finite element mesh of many hundreds of crystallites. Each finite element is a single crystallite having uniform spontaneous

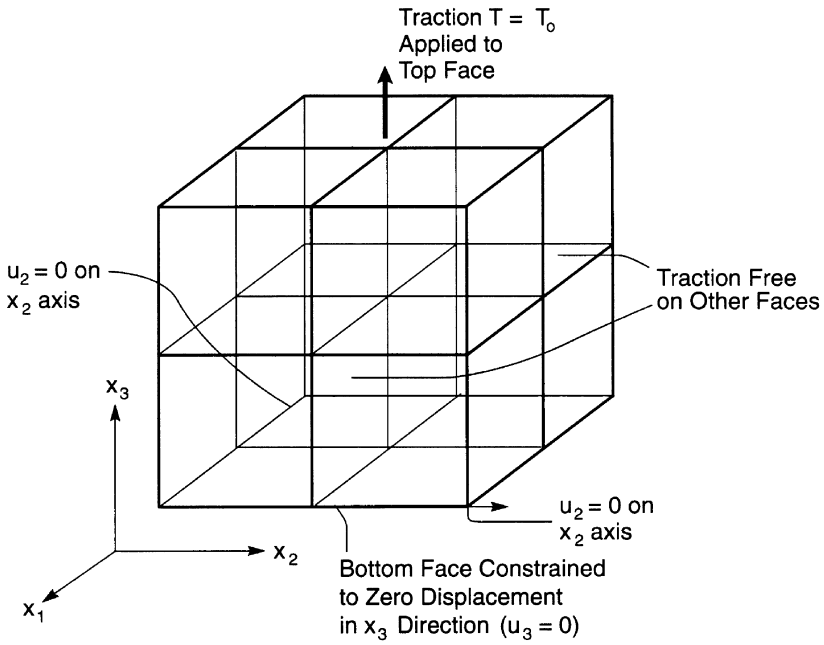

Fig. 1. A schematic diagram of the cubic mesh of eight elements. Each cubic element represents one crystallite and has its own principal crystallographic directions.

strain. A cubic mesh of elements is used for each simulation with each element itself being a cube, as depicted for eight elements in Fig. 1. We use eight-node cubic elements having a node at each corner (Cook et al., 1989). Parallel to the coordinate direction, the elements use a linear interpolation of each displacement component, so that the components have a trilinear dependence on position. A random number generator is used to create the principal axes of the initial tetragonal unit cell of each crystallite. The magnitude of the spontaneous strain of a crystallite parallel to the c-axis of the unit cell is $e_0 = [(c-a_0)/a_0]$. The strain perpendicular to the c-axis is $-\frac{1}{2}e_o = [(a-a_o)/a_o]$, where a_0 is the lattice parameter of a cubic cell having the same volume as the tetragonal cell. In addition, c is the lattice parameter of the tetragonal unit cell parallel to the tetragonal direction and a is the lattice parameter perpendicular to the c-axis. The components of the spontaneous strain of each crystallite are calculated in a fixed Cartesian coordinate system common to the ceramic. These components will be referred to throughout the discussion below.

The macroscopic strain of the aggregate is computed as the volume average of the strain in the crystallites. Since each crystallite has the same volume V_c, the volume average can be computed as a simple arithmetic average of the strain components over all crystallites. Thus, the initial average remanent strain of the polycrystal is zero (or nearly zero because the finite number of crystallites involved in a given simulation can have a nonzero average from the random number generation). Similarly, the average linear contribution to the strain e is zero initially since the imposed traction is zero initially.

The boundary conditions in eqn (15) are imposed such that the displacement u_3 is fixed at zero for all nodal points on the bottom surface of the cubic mesh as shown in Fig. 1 where the x_3 axis

is considered to be vertical and x_1 and x_2 define the horizontal plane. The displacement u_1 is fixed at zero for all points along the lower left edge of the cube and u_2 is zero along the lower front edge. All these nodal points where the displacement is fixed at zero compose S_u. As shown in Fig. 1, the traction is imposed on the top surface of the cube as a uniform value T_3 with T_1 and T_2 equal to zero everywhere except on S_u. The non-zero traction T_3 on the top surface is introduced gradually from zero initially. After a small increment of the traction, each crystallite is checked to see if it has met the switching criterion. The expression for $\Delta\Omega[u]$ given by eqn (22) is substituted into the switching criterion, eqn (6), and is modified in the form:

$$\{\Delta e^s\}^T\{\sigma\} - \frac{1}{2}\{\Delta e^s\}^T[C]\{\Delta e^s\} + \frac{1}{2V_c}\{\Delta F^s\}^T[K]^{-1}\{\Delta F^s\} \geqslant \frac{3}{2}\sigma_0 e_0 \tag{25}$$

where the term $\Delta\psi_c$ is replaced by $\frac{3}{2}\sigma_0 e_0$ with σ_0 being a critical stress with the magnitude of an effective uniaxial coercive stress for a single crystallite parallel to the principal crystallographic directions. The third term on the left hand side of eqn (25) is obtained by combining eqn (22) and eqn (23). The inverse stiffness matrix is computed once only and stored since it does not change during the simulation. Note that $[K]^{-1}$ must be conditioned, as must be $[K]$ in eqn (19) and (23), to account for displacement boundary conditions imposed on S_u (Cook et al., 1989). This is a trivial step since all boundary conditions on S_u involve zero values of displacement components. The switching criterion is evaluated at the centroid of an element with centroidal values of strain, spontaneous strain and stress taken to represent the element as a whole. Since switching is considered for one element at a time, the first two terms on the left hand side of eqn (25) are computed only for the element under consideration for switching. For each crystallite, the tetragonal symmetry dictates two possible ferroelastic (or 90°) switches. At any given stage, the switch which is taken to occur for an element is that associated with the greatest value of the left hand side of eqn (25). After all possible switches have been checked for satisfaction of eqn (25), the element for which the left hand side of eqn (25) exceeds the right hand side by the greatest amount is identified as the one element which will switch.

After a switch has been identified and made, a new load $\{F^s\}$ in eqn (19) is computed by reassembling the spontaneous strains of all the crystallites in the finite element mesh. Solution of eqn (19) with the new $\{F^s\}$ gives new nodal displacement values $\{u_N\}$, and then the stress tensor $\{\sigma\}$ in each element is re-evaluated. With $\{u_N\}$ and $\{\sigma\}$ updated, another permitted switch associated with the greatest value of the left hand side of eqn (25) is sought without change of the prescribed traction. This process is repeated until no more elements will switch. The macroscopic strain for the polycrystal is then computed by averaging the strain over all elements. The traction is then incremented and eqn (25) is used to select further switches. The increments of the traction are chosen so that only one crystallite will tend to switch at any given stage.

It should be noted that the crystallites in their initial state with randomly generated tetragonality have spontaneous strain. This causes incompatibilities which generate residual stress in the polycrystal at the outset of the simulation. The first step is to calculate these residual stresses with zero applied load which requires a solution of eqn (19) with $\{F\}$ equal to zero. The possibility exists that these residual stresses will drive switching by themselves. To allow for this, switches are investigated at zero applied load ($\{F\} = 0$) and are allowed to continue until no more occur spontaneously. The final stable annealed state is taken to be the true initial configuration for

simulations which are then carried out with an applied load increased gradually from zero. Therefore, the initial configuration of the polycrystalline aggregate at zero load for these simulations has residual stress present in them but each crystallite is in a stable state until external load is applied.

The elastic compliance of a single crystallite in general is anisotropic with the c-axis orientation determining the values. Generally, there are insufficient experimental data for moduli values of 8/65/35 PLZT single crystallites. On the other hand, Young's modulus along the poling axis and Poisson's ratio v relative to the same orientation in a poled polycrystalline ceramic are known. Instead of using those values, however, we approximate the elastic tensor C of the crystallites to be isotropic;

$$C_{ijkl} = \frac{Yv}{(1+v)(1-2v)}\delta_{ij}\delta_{kl} + \frac{Y}{2(1+v)}(\delta_{ik}\delta_{jl}+\delta_{il}\delta_{jk}) \tag{26}$$

where Y is Young's modulus. Values for Y and v are chosen to correspond to polycrystalline values.

For hard PZT-A and soft PZT-B ceramics (Cao and Evans, 1993), however, the modulus in the poled direction, Poisson's ratio, and the modulus perpendicular to the poled axis are known. From these data, single crystallite anisotropic elasticity could be estimated to agree with the measured values for the polycrystalline ceramic. If single crystallite anisotropic elasticities were used, the stiffness matrix $[K]$ would have to be reassembled after each switch because the c-axis and one of the a-axis of the switching crystallite will be interchanged, thereby changing C in a fixed coordinate system. Also the inverse of the matrix $[K]^{-1}$ would have to be re-evaluated for the switching criterion after each switch. Inverting the matrix $[K]$ is computationally burdensome. Therefore, to avoid immensely increased computing time, the elastic tensor C of all crystallites in both PZT ceramics are approximated to be transversely isotropic with respect to the direction of applied stress. Then, the tensor C is fixed for every crystallite regardless the direction of its c-axis and no recomputation of $[K]$ or $[K]^{-1}$ is necessary. The experimental poling direction modulus (Cao and Evans, 1993) is used for the computational modulus parallel to the applied stress direction, with the experimental Poisson's ratio and transverse modulus values relative to the poling direction (Cao and Evans, 1993) used for the computational Poisson's ratio and transverse moduli relative to the applied stress axis.

5. Results

All the calculations presented in this paper are done with an identical set of 1000 crystallites with random c-axis orientation. The crystallites, each one represented by a finite element, are in a $10\times10\times10$ cubic array with cube edges parallel to the Cartesian coordinate directions. The numerical results for a simulation for a given random set are mostly within 10% of the values for other simulations abased on a different random set of 1000 elements.

A polycrystalline 8/65/35 PLZT ceramic of 10 mm cube was used to obtain experimental data (Hwang et al., 1995). The initial unpoled state of the PLZT was used as the zero strain state. Several cycles of electric field (±0.8 MV/m) were applied to the sample until a repeatable electric displacement vs electric field hysteresis loop was obtained. After the sample was poled, the field

was then reduced to zero, and compressive stress was applied. The resulting stress–strain curve is used for comparison with the numerical results. The experimental methods used for PZT ceramics were identical to those for PLZT (Hwang et al., 1995; Cao and Evans, 1993). The only difference was that the PLZT was poled in the laboratory whereas poled PZTs were bought from a manufacturer. The sample size of the PZTs was $6 \times 8 \times 12$ mm. In the experiments, the measured value for the modulus in the poling direction is the value of the initial elastic slope of the stress vs axial strain curve when the ceramic is subjected to compressive stress applied along the poled axis; the measured transverse modulus is the value of the initial slope of the stress vs axial strain curve under compressive stress applied perpendicular to the poled axis; the measured Poisson's ratio is the negative of the quotient of the increment of transverse strain and the increment of axial strain under compressive stress applied along the poling axis.

5.1. Simulation of PLZT ceramic

The parameters used are experimentally determined values, $e_0 = 0.00259$ and $Y = 68$ GPa (Hwang et al., 1995). The measured Poisson's ratio value is 0.5, indicating incompressibility. To avoid a singular finite element stiffness, v is chosen instead to be 0.48. Mesh locking (Cook et al., 1989) is avoided by one point numerical integration of the stiffness. The critical stress, σ_0, is selected to be 55, 15, or 1 MPa.

Figure 2 shows the simulation stress versus longitudinal strain loop for σ_0 equal to 55 MPa. The average strain is zero initially because the crystallites have random states of tetragonality. As the applied stress is increased from zero, the strain increases linearly due to elasticity, and then changes its slope significantly at 40 MPa as crystallites switch. The remanent strain reaches its maximum at a stress of 150 MPa. At this stage, all possible switching has taken place and the c-axis of all elements are aligned as closely as possible to the applied stress direction. Increase of stress above 150 MPa causes only further linear elastic deformation. When the stress is decreased, the strain decreases nearly linearly. At a coercive stress of -100 MPa, nonlinear deformation takes place as reverse switching occurs. The remanent strain continues to decrease until it saturates at a stress of

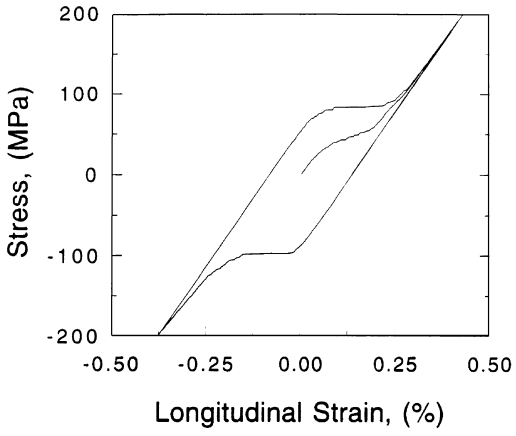

Fig. 2. Simulated 8/65/35 PLZT axial stress vs axial strain hysteresis loops for an effective stress $\sigma_0 = 55$ MPa.

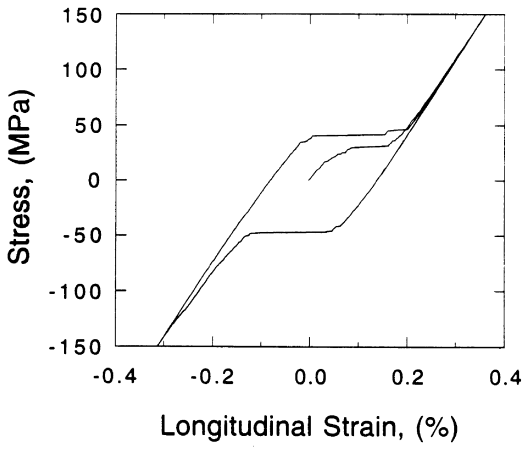

Fig. 3. Simulated 8/65/35 PLZT axial stress vs axial strain hysteresis loops for an effective stress $\sigma_0 = 15$ MPa.

-200 MPa. At this stage, all possible reverse switching has taken place and the c-axis of all elements are aligned as far as possible away from the applied stress direction. Application of further compressive stress causes only linear elastic deformation. The imposed stress is then increased. At a stress of 70 MPa, the ceramic starts deforming nonlinearly back to its elongated state, and the deformation continues until the remanent strain again saturates. Further cycling of the stress will cause a repeat of the same loop. When the applied stress is reduced to zero, there is a remanent strain. It should be noted that the change of the slope near the coercive stress in tension is more gradual than that in compression. Also the absolute magnitude of the coercive stress for the repetitive loop is less for tension (85 MPa) than for compression (-100 MPa).

Figure 3 shows the stress vs longitudinal strain hysteresis loop for σ_0 equal to 15 MPa. The features are similar to Fig. 2. The initial switching (or nonlinear deformation) from the random state occurs at 20 MPa, and the magnitude of the coercive stress under compression drops to 45 MPa, a substantial change from the corresponding value of 100 MPa in Fig. 2. Figure 4 shows the loop for σ_0 equal to 1 MPa, which can be considered as a nominally zero critical stress. The low σ_0 allows the nonlinear deformation in the initial random state to start at nearly zero stress. Once the switching strain saturates, however, the constraint among elements [i.e. the second and third terms on the left hand side of the switching criterion, eqn (25)] plays the dominant role in determining when switching takes place, whereas the right hand side is negligible. Physically, a crystallite in the polycrystal finds it difficult to undergo switching due to the presence of the surrounding stiff crystallites and the inherent barrier to switching is unimportant.

In Fig. 4, the saturated remanent strain at zero stress after a complete cycle of stress reaches only 90% of the corresponding strains in Figs 2 and 3 even though the initial random orientation of the crystallites and the spontaneous strain of crystallites are exactly the same for all these simulations. The reason for this is that a low critical stress ($\sigma_0 = 1$ MPa) as used in Fig. 4 cannot keep the crystallite spontaneous strain fixed after removal of the load. Some crystallites switch to find the lowest energy state for the system by responding to the constraints due to the presence of

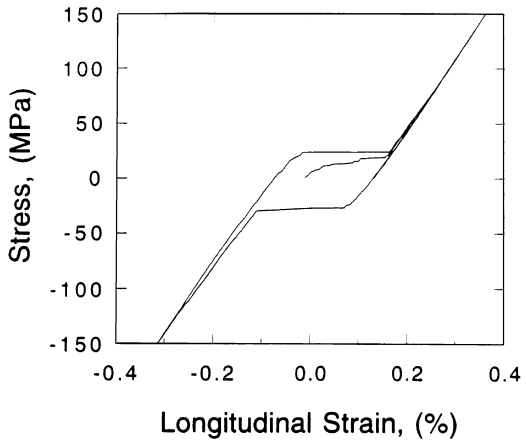

Fig. 4. Simulated 8/65/35 PLZT axial stress vs axial strain hysteresis loops for an effective stress $\sigma_0 = 1$ MPa.

the surrounding stiff crystallites; this adjustment is easier when the energy barrier is low. In addition, it was found that the remanent strain in the unpoled state varied up to 40% in terms of the saturated remanent strain for other simulations based on different random sets of 1000 crystallites. This behavior seems to be due to the unstable nature of the residual state when the barrier to switching is low. On the other hand, once strain saturate, and the stress is high, results for a given random set are within 10% of the values from different random sets even when the energy barrier is low. In addition, when the random crystallites are initially created, the remanent strain is well below 1% of the saturation value. As noted above, the crystallites are allowed to anneal by switching at zero load to find their minimum energy state in the system and in these simulations the strain then usually decreases below zero. The deviation from the zero strain in the unstressed initial state in this process is large when the effective stress σ_0 is low (i.e. 1 MPa).

Figure 5 shows the axial stress vs longitudinal strain for PLZT with the experiment represented by the thin line and the calculation represented by the bold line. The calculated curve is identical to that in Fig. 4 with $\sigma_0 = 1$ MPa, but only the segment in the compressive stress stage is presented in Fig. 5. The simulation shows reasonable agreement with the experiments except that the gradual depolarization of the experimental curve is not matched well. After stress is applied and removed, the remanent strain of the simulated curve is somewhat larger than that of the measured curve. This mismatch suggests that the correct crystallite spontaneous strains have not been used in the simulation. Indeed, the version of PLZT used in the experiments has a significant amount of rhombohedral material in it, which may explain the discrepancy (Hwang et al., 1998). Another source for the error could be the neglect of crystallite anisotropic elasticities.

The experimental data show also that switching occurs gradually at low stress. This phenomenon does not appear in the finite element model because of a strong constraint effect which inhibits switching at first. However, it is possible that this deficiency is due to the small size of the simulation (1000 elements). In a larger model, some elements would be favorably disposed to switching because of the influence of near neighbors and this might reproduce the initial switching in the experimental curve of Fig. 5.

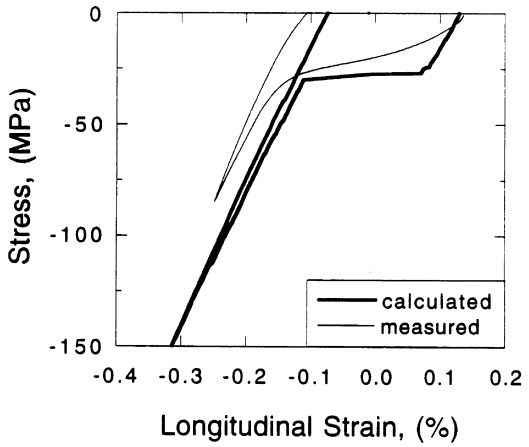

Fig. 5. Simulated 8/65/35 PLZT axial stress vs axial strain curves in compression after nonlinear elongation. The simulated curve has an effective stress $\sigma_0 = 1$ MPa.

5.2. Simulation of PZT ceramics

The simulation is fitted also to experimental data for polycrystalline PZT ceramics. It is found that a best fit to the stress vs strain curves of hard PZT-A and soft PZT-B (Cao and Evans, 1993) can be obtained with $\sigma_0 = 1$ MPa and $e_0 = 0.0808$. The zero strain datum of the original experimental data corresponds to the poled state (Cao and Evans, 1993), whereas the zero strain corresponds to the initial unpoled state in all our previous results. Thus, 0.38% strain was added to the experimental data to match the zero strain to that of the simulation. This is an arbitrary step since the strain of the poled PZT samples relative to the unpoled state is unknown. Other values used for parameters are 133 GPa for the modulus parallel to the poling axis, 82 GPa for the modulus transverse to the poling direction, and 0.4 for Poisson's ratio for PZT-A and 133 GPa (poling modulus), 64 GPa (transverse modulus), and 0.4 (Poisson's ratio) for PZT-B. It is notable that all parameters with the exception of the transverse modulus are the same for simulating both hard and soft PZT ceramics. The poling modulus has been chosen to provide good agreement between the simulations and the experiments in the linear response regime. One complete axial stress vs strain loop each for PZT-A and PZT-B is generated, but only the part of the curve under compression is presented.

Figure 6(a) shows the simulated and measured stress vs strain curves for hard PZT-A ceramic (Cao and Evans, 1993) and Fig. 6(b) shows the stress vs strain curves for soft PZT-B ceramic (Cao and Evans, 1993). Both simulations show generally good agreement with the experiments. As with the simulation for PLZT, the gradual process of switching in the early stage of the stress–strain curve is absent in the calculated curves. Also the simulation does not show any significant strain recovery as observed in the experiments. (Note that in experiments, crystallites in a hard ceramic are more likely to switch back to their previous orientations than those soft materials.) However, the enlargement of the transverse modulus from 64 GPa for PZT-B to 82 GPa for PZT-A increased

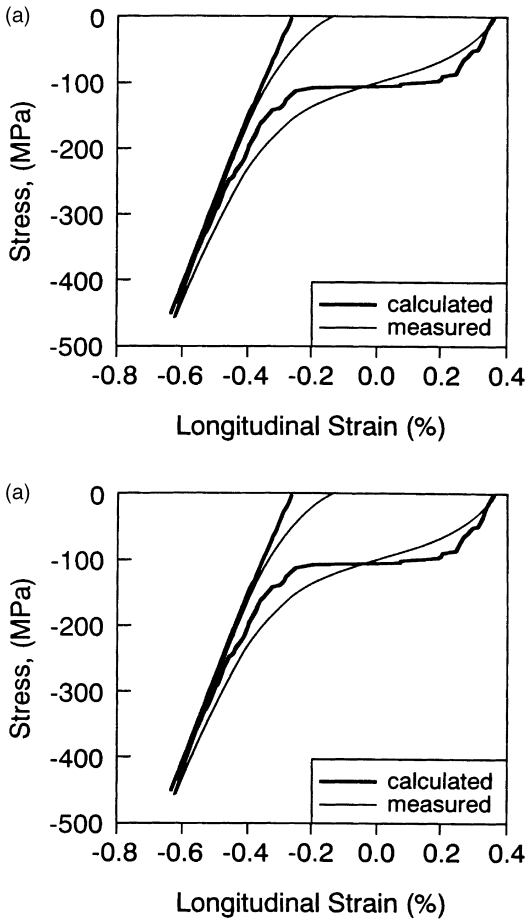

Fig. 6. Simulated and measured PZT axial stress vs axial strain curves in compression after nonlinear elongation. The experimental curves are for a material which was electrically poled. The simulated curves are both for an effective stress $\sigma_0 = 1$ MPa. (A) Hard PZT-A. (b) Soft PZT-B.

the coercive stress level by approximately 10 MPa. Other than this difference in the coercive stress level, both simulations are similar to each other.

6. Discussion

In these simulations, the significant differences between the critical stress value σ_0 in the computations and the coercive stress measured in experiments is due to the presence of the second and third terms on the left hand side of eqn (25). If the material were a single crystallite, the third term on the left hand side of eqn (25) would be zero, and the single crystallite would switch at or near the critical stress level. Since the simulations agree best with the experiments when $\sigma_0 = 1$ MPa, it can be deduced that the inherent energy barrier to switching in crystallites is very low. The third

term on the left hand side of eqn (25) is present due to constraint arising from the interaction with neighboring crystallites. This effectively increases the energy barrier for a switch in a ceramic. Switching in an unpoled polycrystal initiates relatively easily at low stress (see Figs 2–4) indicating that the constraint among randomly aligned crystallites is modest. The more severe constraint due to surrounding crystallites comes into effect after nonlinear deformation has been induced and the crystallites have been aligned as much as possible. The reason for this is that the near alignment of the c-axis of the crystallites makes it more difficult to switch the first crystallite out of the aligned configuration. However, after one crystallite is switched, the constraint on the next crystallite to switch is reduced somewhat. Thus, the constraint diminishes steadily as switching proceeds. The result is the rather abrupt transition (i.e. the nearly perfectly plastic behavior) in the simulations at the effective coercive stress.

In principle, it would be possible to enlarge the simulation and carry out calculations for many thousands or tens of thousands of crystallites. However, the approach described here involves a computational effort which increases approximately with n^2 where n is the number of crystallites in the simulation. This occurs because the procedure requires each crystallite to be checked for its tendency to switch at each incremental step of the calculation. Such an escalation of computational burden makes this scheme unattractive for larger scale simulations such as the behavior of crystallites near a crack tip under strain. However, the results of calculations such as those described in this appear can be used to guide the development of macroscopic constitutive laws for the behavior of polycrystalline aggregates. Such macroscopic constitutive laws are more likely to be useful for the computational modeling of problems such as the behavior at crack tips.

7. Conclusions

A finite element method with each crystallite represented by an element which transforms completely upon switching can be used to model ferroelastic behavior of polycrystalline aggregates. A criterion in which the reduction of the system total potential energy is equal to or greater than an energy barrier is found to be suitable for determining when individual crystallites switch. The energy barrier to switching required to match the simulations to experimental data for PLZT and PZT is found to be very low, equivalent to a coercive stress of 1 MPa for a single crystal sample. Most of the resistance to switching in a poled polycrystal in the simulations is then found to be due to elastic constraints among the residually stressed crystallites. The simulation successfully models PLZT and PZT with the difference between these two materials being due to the spontaneous strain magnitude and elastic anisotropy rather than the size of the barrier to switching.

Acknowledgments

This work was supported by ONR through contract N00014-93-1-0200. We wish to thank Dr Xiaoyun Gong and Professor Zhigang Suo for many helpful discussions and thank Dr Hengchu Cao of Carbomedics, Inc. for providing us with experimental data.

References

Aburatani, H., Harada, S., Uchino, K., Furuta, A., 1994. Destruction mechanism of ceramic multilayer actuators. Jpn. J. Appl. Phys. 33, 3091.

Cao, H., Evans, A.G., 1993. Non-linear deformation of ferroelectric ceramics. J. Am. Ceram. Soc. 76, 890.

Chan, K.H., Hagood, N.W., 1994. Modeling of nonlinear piezoceramics for structural actuation. In Hagood, N.W. (Ed.), Proc. SPIE, Smart Struct. Mat. 2190, 194.

Cook, R.D., Malkus, D.S., Plesha, M.E., 1989. Concepts and Applications of Finite Element Analysis. John Wiley and Sons, New York.

Duerig, T.W., Melton, K.N., Stoectsel, D., Wayman, C.M., 1990. Engineering Aspects of Shape Memory Alloys. Butterworth-Heinemann, Boston.

Hwang, S.C., McMeeking, R.M., 1998. A finite element model of ferroelectric polycrystals. Ferroelectrics, in press.

Hwang, S.C., Lynch, C.S., McMeeking, R.M., 1995. Ferroelectric/ferroelastic interactions and a polarization switching model. Acta Metall. Mater. 43, 2073.

Hwang, S.C., Huber, J.E., McMeeking, R.M., Fleck, N.A., 1998. The simulation of switching in polycrystalline ferroelectric ceramics. J. Appl. Phys., in press.

Jaffe, B., Cook, W.R., Jaffe, H., 1971. Piezoelectric Ceramics. Academic Press, London and New York.

Jiang, Q., Cao, W., Cross, L.E., 1994. Electric fatigue in lead zirconate titanate ceramics. J. Am. Ceram. Soc. 77, 211.

McMeeking, R.M., Evans, A.G., 1982. The mechanics of transformation toughening in brittle materials. J. Am. Ceram. Soc. 65, 242.

McMeeking, R.M., Hwang, S.C., 1997. On the potential energy of a piezoelectric inclusion and the criterion for switching. Ferroelectrics 200, 151 .

Park, S., Sun, C.T., 1995. Fracture criteria for piezoelectric ceramics. J. Am. Ceram. Soc. 78, 1475.

Wang, Y., Gong, S.-X., Jiang, H., Jiang, Q., 1996. Modeling of domain pinning effect in polycrystalline ferroelectric ceramics. Ferroelectrics 182, 62.